Elastic characterization of nanometer-thick polymeric film for astrophysics application with an experimental-numerical method

Nicola Montinaro [a,b,c,d,*] **Ugo Lo Cicero,** [d] **Fabio D'Anca,** [d] **Enrico Bozzo,** [c] **Stéphane Paltani,** [c] **and Marco Barbera** [d,e]

[a]Università degli Studi di Palermo, Dipartimento di Ingegneria, Palermo, Italy
[b]Institute for Advanced Energy Technologies (ITAE), National Research Council, Palermo, Italy
[c]Université de Genève, Département d'astronomie, Faculté des sciences, Genève, Switzerland
[d]INAF-Osservatorio Astronomico di Palermo, Palermo, Italy
[e]Università degli Studi di Palermo, Dipartimento di Fisica e Chimica, Palermo, Italy

ABSTRACT. The x-ray detectors on board astrophysics space missions require optical blocking filters that are highly transparent to x-rays. The filter design typically consists of a polymeric film that is a few tens of nanometers thick coated with aluminium. Due to the large size of the filter membrane (from a few tens to a few hundred square centimeters) and the extreme aspect ratio, together with severe loading conditions during launch and different stoichiometries of the polymer that could change its mechanical properties, a characterization study of the employed material is needed. The plane strain bulge test is a well-accepted methodology for the mechanical testing of structures that are less than a micrometer thick, and especially for free-standing membranes. Unfortunately, testing such ultra-thin films is not a simple task due to residual stress and experimental uncertainty at very low pressure. In this work, the elastic properties of an extremely thin (between 45 and 415 nm) membrane made of bare polyimide and coated with aluminium were derived through adopting a combined experimental-numerical methodology based on the bulge test and numerical simulations.

1 Introduction

The x-ray astrophysics future missions require an increase in the in-band transparency of the optical blocking filters (OBF) to fully exploit new detectors' sensitivity.[1–3] This implies the adoption of increasingly thin membranes. The OBFs are required to block infrared to ultraviolet light and molecular contamination and to attenuate the electromagnetic interference originated by the telemetry system and the instrument electronics. The large-class astrophysics space mission "Athena" (selected by European Space Agency in the Cosmic Vision 2015–2025) will be equipped with an x-ray telescope and two interchangeable focal plane instruments named X-ray Integral Field Unit (X-IFU)[4] and Wide Field Imager.[5] Both instruments will need filters that need to be extremely thin to maximize x-ray transparency, just a few tens of nanometers, and be made of low atomic number materials; the baseline adopted for the Athena filters is a thin layer of

---

*Address all correspondence to Nicola Montinaro, nicola.montinaro@unipa.it

polyimide (PI) coated with Al (a low-Z metal). Despite the very small thickness, filters are required to survive severe mechanical stresses. Specifically, the X-IFU thermal filters are operated at low temperatures inside a vacuum cryostat; for this reason they have to be able to survive small static differential pressure loads that may build up during venting/filling procedures in laboratory tests. In addition, during the launch, they will have to withstand severe vibration loads generated by the rocket boosters while they are at room temperature, either in vacuum or in a moderate gas pressure (TBD) inside the cryostat enclosure. The wide field imager (WFI) OBFs will be launched in atmospheric pressure and, for this reason, they will have to withstand simultaneously the vibration loads and the powerful acoustic spectrum transmitted inside the launcher cargo.[6]

The nanometric film thickness and the severe static and dynamic loading conditions, combined with the existence of different PI stoichiometries that could change the mechanical properties, need a characterization of the membrane material. The modification of the material properties moving from bulk to thin sheets and the dependence of the mechanical properties on the microstructure (grain size, texture, and defects) are studied topics.[7–9] A strain characterization of the film material is also useful for predicting the nucleation of fine cracks in the Al coating, potentially leading to mechanical failure and light leakage.

The plane strain bulge test has become a generally accepted methodology for mechanical characterization of structures less than a micrometer thick, and especially of freestanding membranes, under various thermodynamic conditions.[10–13] Among other testing methods, the bulge test technique provides significant flexibility in terms of the range of stress/strain states to which a sample can be subjected. The main benefits are an easiness of loading conditions and a minimal sample handling, which is challenging with extremely fragile samples. These advantages are unparalleled by other thin film testing methods, such as nanoindentation[14,15] and microtensile testing.[16–20]

However, the uncertainty on the initial conditions of a film subjected to a bulge test can lead to inaccurate predictions. Specifically, the assumption of an initially flat, unstressed film is unrealistic, especially for ultra-thin films that are prone to developing residual stress, leading to slack or stretched membranes at rest conditions.[21] This is the case for PI thin films, in which the remarkable hygroscopicity contributes to either relaxation or pre-stress (stretched or slack membrane), depending on the manufacturing and test conditions.[22] The effect of a slack membrane on the elastic properties could be taken into account in analytical calculations; however, the initial deflection of the film (at infinitesimal differential pressure) must be acquired with high precision. It is a matter of fact that a precise acquisition of the initial deflection of nanometric thick films is not a simple task because a minimal fluctuation of the pressure (of just few μbar) can affect the results. If the initial deflection is accurately known, this data could be used as an input in the predictive models[23–30] and then used to calibrate the pressure-deflection data. However, each analytical formulation can be applied only to a specific case with fixed geometry to preserve accuracy, due to the basic assumption of the model.

A more attractive and accurate method to model the bulged film is the finite element analysis (FEA). The adoption of numerical models allows for overcoming any analytical model constraint, ensuring maximal flexibility of the solution while preserving accuracy.

With the FEA model, all of the boundary conditions are accurately simulated, and the elastic properties are determined with an optimized workflow, after performing a series of parametric simulations to fit the experimental data. This experimental-numerical approach is interesting, especially in the case of material non-linearity, anisotropy, irregular test windows (not circular or square), and uncertainty in the initial conditions. Furthermore, the FEA can be used to study the stress–strain behavior of the membranes and eventually of the coatings.[31,32]

A mechanical characterization study of Al-coated thin PI film (with thickness ≥0.5 μm) using the bulge test technique can be found in Ref. 33. The same approach has also been used to test the deflection versus the differential pressure of ultra-thin Al-coated PI membranes reinforced with a metal mesh for aerospace applications.[34,35] The bulge test has been adopted to mechanically characterize composite bi-layer membranes and coatings over a substrate.[20,31,35,36] In Ref. 37, the tenacity of 500 nm thick PI films at varying temperatures was measured by applying a burst pressure method. In Ref. 38, the elastic modulus of Al-coated films (with Al thickness > 150 nm) was evaluated by means of two laser optical measurement

techniques: a test approach based on a microscale beam combined with FEA and a picosecond ultrasonics wave propagation analysis. No investigations have been found in the literature, to the authors' knowledge, on bulge mechanical characterization of PI film and Al-coated PI film with thicknesses < 150 nm, which is relevant for filter applications on soft x-ray/extreme ultraviolet (EUV) astrophysics space missions.

In this paper, the elastic properties of extremely thin (between 45 and 450 nm) membranes, made of bare PI and coated with Al, were derived adopting an experimental-numerical approach, combining experimental measurements with a tailored set of numerical simulations. The novelty lies in the use of the initial height as a simulation parameter to fit the experimental data, which is necessary because, for the first time, we are dealing with ultra-thin PI films. The approach offers a broader range of applications, and its use, under challenging physical and numerical conditions, demonstrates its reliability and stability.

2 Material and Methods

2.1 Samples

The tested samples, bare and Al-coated PI, are representative of the thermal filters that will operate inside the X-IFU cryostat.[4] Overall, 14 samples with different geometries of the substrate and coating, varying both diameters and thicknesses, were tested, to retrieve the elastic properties of the materials. The PI films tested were biphenyldianhydride/1,4 phenylenediamine (BPDA/PPD) with stoichiometry $C_{22}H_{10}N_2O_4$. In all samples, the membrane is glued to a two-part Al frame that mechanically supports it (see Fig. 1). In Table 1, a summary of the geometric specifications and the adopted nomenclature for the 14 tested samples is shown. The company Luxel Corporation manufactures the sample assembly (made of an external frame, an inner frame, and the film) using a precision process to control the membrane thickness with very low tolerances (± 3 nm). The tested membranes are from different production batches as shown in Table 1.

2.2 Basic Theory of the Bulge Test

The bulge test is analogous to the tensile test for bulk materials and was developed to derive the mechanical properties of thin films. In the bulge test, a freestanding thin film window is loaded with a differential pressure, causing a deflection (Fig. 2). A stress–strain curve can be determined by measuring the bulge pressure P_i and the film maximum deflection h.

A simple formulation can be used, assuming a spherical geometry for the displaced membrane. Considering the thickness of the film (t) and the bulge radius of curvature (R), the stress in the wall is obtained by a simple force balance as

$$\sigma = \frac{PR}{2\,t}. \tag{1}$$
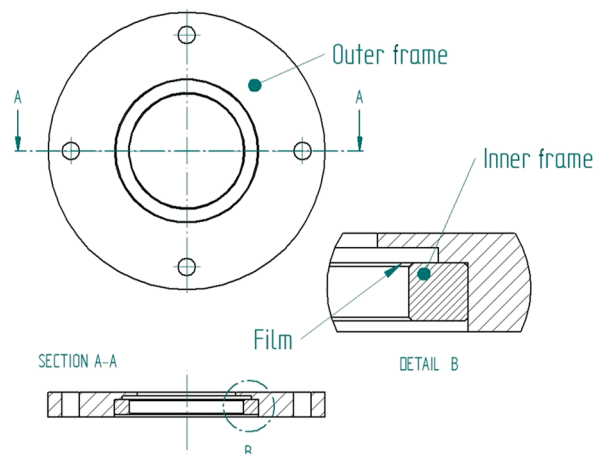
Fig. 1 Drawing of a sample assembly with its three parts: film, inner, and outer frames.

Table 1 Specifications of the 14 tested samples.

Bare PI samples

	Sample 1	Sample 2	Sample 3	Sample 4	Sample 5	Sample 6	Sample 7
Film diameter (D) (mm)	11.8	11.8	11.8	11.8	17.4	11.8	11.8
PI thickness (t) (nm)	47	47	47	148	153	45	415
Production batches		Batch 1		Batch 2	Batch 3	Batch 4	Batch 5
Nomenclature	S1 ($D_1\ t_1$)	S2 ($D_1\ t_1$)	S3 ($D_1\ t_1$)	S4 ($D_1\ t_2$)	S5 ($D_2\ t_2$)	S6 ($D_1\ t_1$)	S7 ($D_1\ t_3$)

PI coated with Al samples

	Sample 1 alum.	Sample 2 alum.	Sample 3 alum.	Sample 4 alum.	Sample 5 alum.	Sample 6 alum.	Sample 7 alum.
Film diameter (D) (mm)	11.8	11.8	17.4	11.8	11.8	11.8	11.8
PI thickness (t) (nm)	47	47	150	148	151	151	152
Al thickness (t) (nm)	29	29	31	30	98	98	197
Production batches		Batch 6	Batch 7	Batch 8		Batch 9	Batch 10
Nomenclature	S1al ($D_1\ t_1\ t_1$)	S2al ($D_1\ t_1\ t_1$)	S3al ($D_2\ t_2\ t_1$)	S4al ($D_1\ t_2\ t_1$)	S5al ($D_1\ t_2\ t_2$)	S6al ($D_1\ t_2\ t_2$)	S7al ($D_1\ t_2\ t_3$)
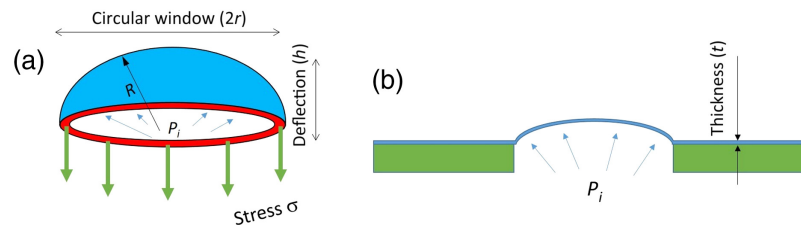
Fig. 2 (a) and (b) Schematic representation of the bulge test for circular window; the green arrows in panel (a) represent the stress σ applied on the annular red area.

In the hypothesis of small deflection ($h \ll r$), the tested material is far from its yielding point, and after some easy geometry calculation, the bi-axial modulus M of the material is found as

$$M = \frac{3P\,r^4}{8\,t\,h^3}.\tag{2}$$

The elastic modulus E is calculated from the bi-axial modulus, knowing the Poisson ratio ν, as

$$E = M(1 - \nu).\tag{3}$$

A detailed explanation of all of the calculations can be found in Ref. 10. Equations (1) and (2) for circular windows allow for determining the bi-axial elastic modulus of a flat membrane from each couple of values of $P - h$ (pressure versus bulge height), with some approximations. The simple model is valid for one layer with a circular window, and with some changes also with a square or rectangular window, but only for small deflections and a flat surface. An initial deflection of the film can be considered in the simple model, to some extent, but with high deflections, the constraints of the model lead to inaccurate predictions.
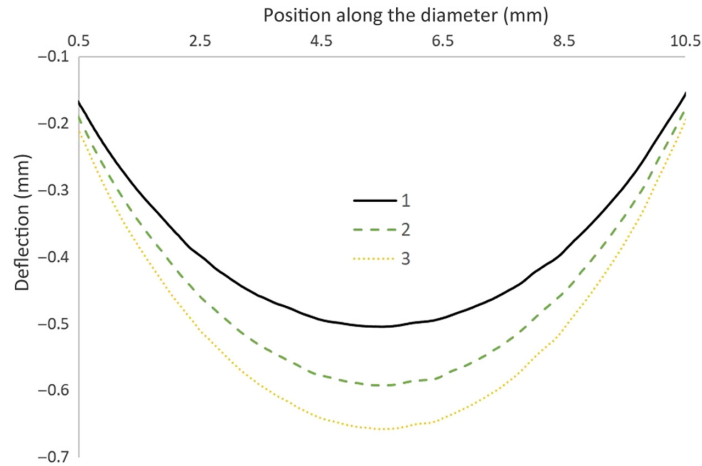
Fig. 3 Bulged profiles of the S1 (D_1 t_1) loaded with 3 pressure levels (solid black 1 mbar, dotted green 2 mbar, and fine dotted yellow 3 mbar). The deflections on the plot are negative values because they refer to the distance from the optical lens that is reduced when the bulge increases.

In Fig. 3, a comparison between three deflected profiles of the same sample (S1), loaded with three different pressure levels (1, 2, and 3 mbar), is shown. The acquisition is performed along the diameter of the membrane, maintaining a fixed value of the static differential pressure. The deflection as a function of the scanline distance (along its diameter) is reported in the plot.

To derive a survivability model for the filter membrane, a study on the elastic and plastic responses of both parts of the membrane (the PI and the Al), as well as a failure analysis after breakage, must be performed. This paper investigates the elastic behavior of the membrane in the Hook's law range because only non-destructive tests are allowed at this characterization stage. Further studies will be carried out on the rheology and failure mechanism of the membranes once optical and thermal characterizations are done, allowing for destructive tests in which filters are under maximum tensile stress.

To avoid applying any plastic deformation to the tested film, the material was kept far below its estimated yielding point.

In Fig. 4, the expected strain level for two different diameters ($D_1 = 11.76$ mm and $D_2 = 17.35$ mm) for the PI is calculated using Eq. (4). This estimation of the strain assumes a flat membrane; thus it is conservative for a slack film and optimistic for a stretched one. Note that Eq. (4) does not depend on film thickness t, assuming that the entire cross section is uniformly stretched:
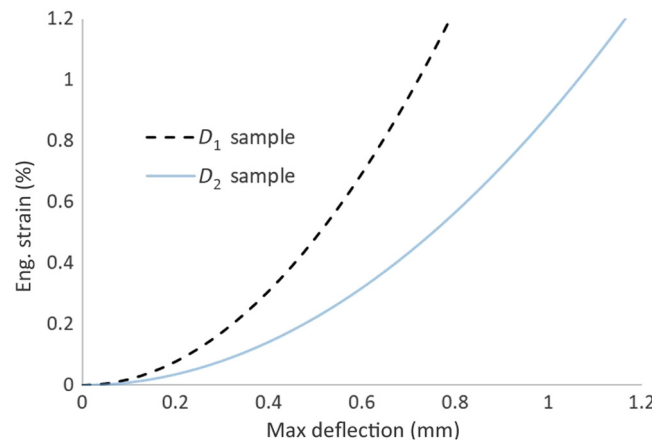
Fig. 4 Expected engineering strain as a function of the deflection for the two samples with the smaller and larger diameter D_1 (11.76 mm) and D_2 (17.35 mm).

$$\varepsilon = \frac{2\,h^2}{3\,r^2}. \tag{4}$$

The upper limit value of strain is $\sim$1% (in accordance with the Kapton® EN datasheet and the Upilex®- S-12.5 datasheet) corresponding to $h \sim 0.7$ mm for the D_1 sample and $h \sim 1.1$ mm for the D_2 samples.

2.3 Experimental-Numerical Approach

The elastic properties of the nanometric membrane were derived after acquiring the experimental deflection with bulge test data and performing a set of FEA analysis, by adopting a reverse modelling approach. A description of this approach for a single-layer membrane is detailed in what follows.

A set of $P - h$ values was acquired with the bulge test for each sample (see Sec. 2.4 for details on the experimental setup), resulting in an experimental curve.

For each of the four combinations of film geometries under test $(D_1\,t_1)$, $(D_1\,t_2)$, $(D_2\,t_2)$, and $(D_2\,t_1)$, a parametric FEA model was generated.

The input parameters for the slack membrane are the initial height h_i and bi-axial modulus M_j, and for the stretched membrane, the parameters are the initial pre-stress hp_i and bi-axial modulus M_j. All are varied in discrete steps, producing an array of solutions with dimensions (i, j). From each computational solution, the pressure versus bulge height curve $(P - h)_{ij}$ is extracted. With the help of an algorithm (executed in Python), the experimental pressure–height $(P - h)$ curve is then compared with the simulated $(P - h)_{ij}$ solutions to generate a "fitness" map, where each element of the array is the inverse of the square differences between experimental and simulated values. This map is called Σ.

The global minimum value of the Σ map is considered the best fit value for the combination of the initial height h_i and bi-axial modulus M_j (or initial pre-stress hp_i and bi-axial modulus M_j) for the corresponding sample. An interpolation could be made on the map data to obtain values for h and E with a better precision than the map resolution.

2.4 Numerical Model

A static non-linear numerical model, simulating the deformation of the film due to differential pressure, was developed using ABAQUS® software. Because a large number of simulations were performed, special attention was paid to reducing the computational effort for the model. Exploiting the structural symmetry of the membrane, a 2D axisymmetric model with shell elements (CAX4 4-node bilinear element) was adopted to define a revolution surface about the medial axis of the film. Shell elements take into account the thickness in their mathematical formulation. The simulation was performed by fixing the perimeter position to reproduce the real boundary conditions during the test. The pressure was applied gradually, step by step, on the film surface, avoiding the emergence of convergence issues due to geometric non-linearity. A preliminary convergence study was performed to fine-tune the model. The final simulations were done using 1630 elements for the smaller samples with diameter D_1 and 2406 elements for the larger ones with diameter D_2. The computation was run on a consumer desktop PC with a CPU Intel i7 4770 and 16 GB random access memory (RAM), resulting in a total time between 60 and 90 min to complete a single set of $(P - h)_{ij}$ solutions, thus a single Σ map.

A pre-test step is required to simulate the slack film (with an initial height $h_i > 0$), to overcome incoming convergence issues due to buckle instability of the thin film.[10] The strategy to model the membrane slackness or pre-stress is to displace the outer edge (on the film perimeter) inward (for slack film) or outward (for pre-stressed film) while a small pressure is applied to the film. The displacement is on the order of a few micrometers. The boundary conditions on the rest of the model remain fixed. A small pressure load is needed during this pre-step to ensure that the film reaches the desired height without any buckle instability. The pressure is then gently released, leaving the film with the desired initial height h_i (in the case of slack film) and ready for the load-deflection run. In the case of simulations of bilayer membranes (coated PI), a perfect adhesion interaction between the coating and the substrate was assumed.
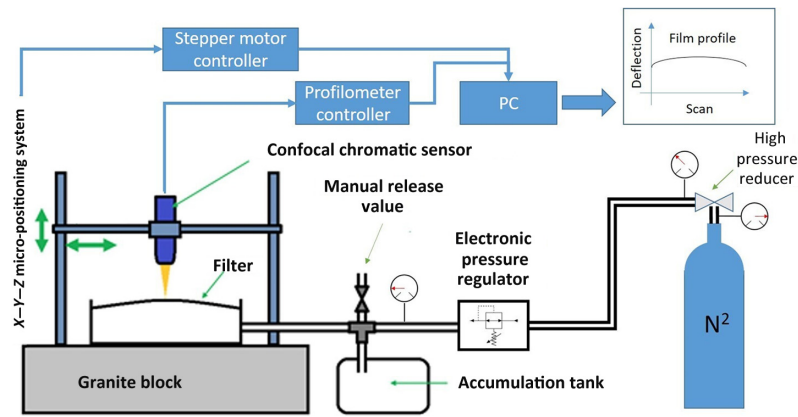
Fig. 5 Schematic representation of the experimental setup.

3 Bulge Test Setup

The experimental setup comprises an XY-translator to move the filter along its plane, an optical sensor to measure the film deflection, a sample-holder, and a pressurizing system to apply a controlled differential pressure (see Fig. 5). The filter is mounted on a custom sample holder and sealed to the filter frame with an o-ring to allow for pressurization of the bottom face. The sample holder is attached to the computer-controlled translator, which moves the bulged filter to measure the membrane profiles with the sensor.

The pressurizing system adopts a precise electronic pressure regulator (Equilibar® model QPV) and a couple of manual pressure reducing regulators (at high- and low-pressure stages) connected to a pressurized nitrogen tank. The pressurizing system compensates for gas leaks, regulating the set pressure with an accuracy of 0.17 mbar, while a manometer measures the actual differential pressure between the two sides of the membrane (Chauvin Arnoux model CA852 with resolution of 0.275 mbar and accuracy ±0.3% full scale). The scanning of the sample is performed along one of its diameters while the differential pressure is kept constant for the duration of the acquisition. The displacement measurement system is a Micro-epsilon® optical confocal sensor system, which comprises the controller (model confocal DT 2421) and the sensor head (model IFS 2405-10), which are connected with an optic fiber (see Table 2 for the main specifications of the system). The measurement principle is based on the projection of polychromatic light (white light) on the target surface. The device optics are designed to use controlled chromatic aberration to focus each light wavelength at a specific distance. The head receives the light reflected from the target surface and transfers it to the controller. A spectral analysis follows, and data stored in the controller is used to calculate distances. This system allows for high accuracy in the displacement measurement and good resolution along the filter plane due to the small beam spot diameter. However, measurement deviations may occur if the measured structure is of a similar size to the beam spot or if the maximum tilt angle is exceeded.

Particular care was taken in setting the scan parameters, such as scan speed, sampling frequency, and peak selection threshold, to pursue a reliable profile measurement. It is worth noting that a bare PI film with sub-micron thickness is nearly transparent in visible light, thus affecting

Table 2 Main specification of the confocal chromatic sensor connected with its lens adopted in the bulge test experiments.

Optical sensor model IFS 2405-10	
Measuring range	10 mm
Spot diameter	16 μm
Resolution	60 nm
Max. tilt	±17 deg

the signal-to-noise ratio of the instrument. The scan speed is a trade-off between the duration and the stability of the measurement; a reasonable value was found to be 1 mm/s. The high sampling frequency (1 kHz) of the acquisition would allow for increasing the scan speed but the floating window averaging was preferred instead to reduce the noise on the two extreme sides of the profile (at the beginning and end of the scan) due to the tilted position of the film with respect to the beam (at higher deflections). All of the acquisitions were performed in a controlled environment with typical temperature and humidity values of $T = 24°C$ and relative humidity (RH) = 60% in an ISO 7 clean room, respectively.

4 Results

4.1 PI Film Elastic Characterization

The experimental-numerical approach described is used to calculate the elastic properties of ultra-thin PI films.

The experimental $P - h$ curve for each sample is compared with the simulated solutions $(P - h)_{ij}$ generating a 2D fitness array Σ. Each element of the Σ_{ij} represents the inverse of the square differences between the experimental and simulated ones obtained with the initial height h_i (mm) and the bi-axial modulus M_j (GPa).

The resolution of the Σ maps is a trade-off between computation time and result accuracy, considering that there are experimental uncertainties that effectively limit the attainable accuracy. Specifically, the effect of the uncertainty on the film thickness (± 3 nm) has a significant effect on the results. For thinner films (S1, S2, S3, and S6 with $t = 47$ nm), the thickness uncertainty could affect the elastic modulus up to 10%, whereas the thicker films are less influenced: <3% for S4 and S5 and <1% for S7. Moreover, some experimental uncertainty is mainly due to the pressure measurement and in small part to the bulge height measurement. The selected bi-axial modulus step is 0.75 GPa, and the initial height step is in the range 4 to 12 μm depending on the sample diameter.

The Σ maps for the S1, S2, and S3 samples, all with the same geometry (D_1, t_1), and for the S5 sample, with a larger diameter and thickness (D_2, t_2), are shown in Fig. 6. Both the diameter of the circles and the color scale represent the fitness of the solution, with different scales to enhance visibility.

By looking at the Σ maps, a global maximum value for each case is found. The bi-axial modulus for the samples range between 16 GPa (for S1, S2, and S6) and 14.4 GPa (for S3), and the initial heights found are all around 0.145 ± 5 μm for the smaller diameter D_1. Because sample S5 has a larger diameter D_2, a higher value of the initial height is expected.

By looking at the maps in Fig. 6 and observing the diameter of the circles (which are proportional to the fitness), there seems to be a set of parameter combinations, linearly arranged in the height-modulus space, that all show similar fitting values. The color scale was obtained by rescaling the fitting values with a power law to mark the differences between close values and to highlight the maximum. The result is significantly more sensitive to the initial height parameter than to the elastic modulus, as can be observed from the scale of the plot. A best-fit zone is grouped in a diagonal line starting in the bottom-left corner, through the maximum value, ending in the top-right corner, and vice versa, moving along the other diagonal (from bottom-right to upper-left), the trend is very steep (with a higher first derivative). This pattern shows how important the acquisition of the initial height is to determine the elastic modulus in such thin structures.

Similar Σ map trends were found for the S4 $(D_1 t_2)$ and S6 $(D_2 t_1)$ samples, whereas in the case of the thicker S7 $(D_1 t_3)$, a pre-stress on the membrane was found instead of a slackness.

Table 3 shows a summary of the initial height, bi-axial modulus, and elastic modulus (assuming a Poisson ratio ν of 0.34 in accordance with the Kapton® EN datasheet) obtained for each of the bare PI samples. Considering that, the slacker a membrane is, the more it can withstand deformation (in terms of initial height) without experiencing any internal stress (Stress = elastic moduli × strain → $\sigma = E\varepsilon$ in the Hook's region), an apparent strain can be used as an indicator of the slackness. This apparent strain can be calculated for each film geometry using Eq. (4), using the initial height in the numerator. In this work, this dimensionless indicator is named the slackness factor and is reported in Table 3 for all of the samples.
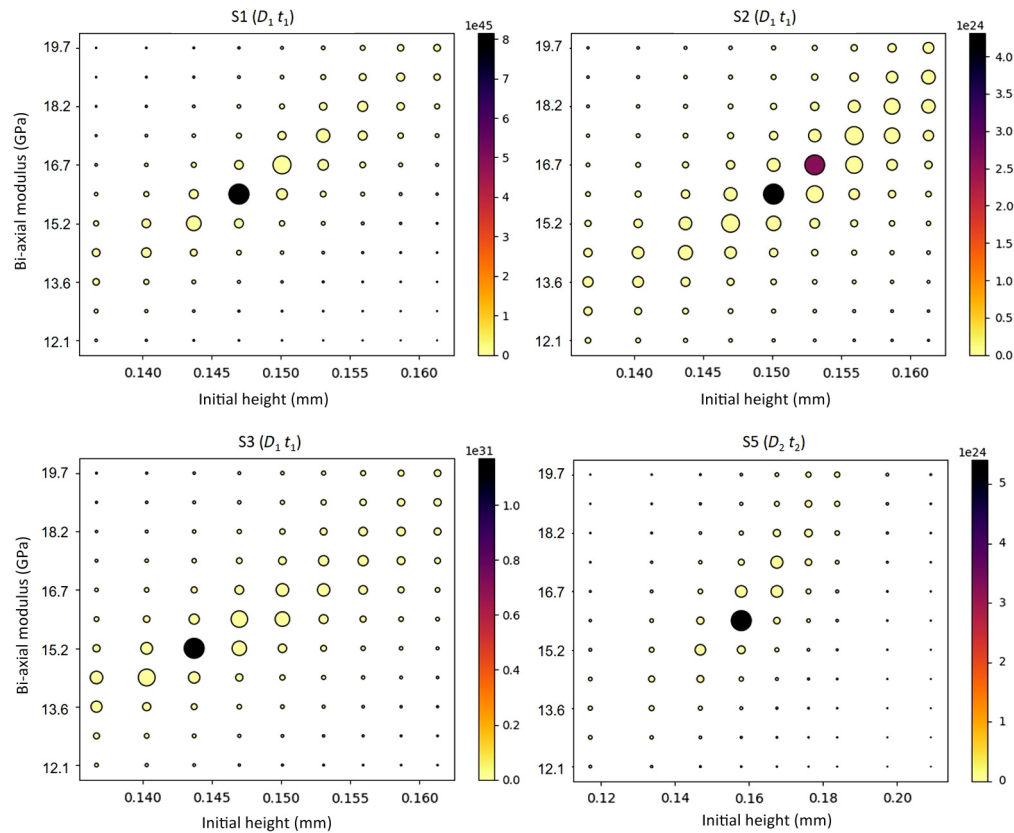
Fig. 6 Representation of Σ map for the S1, S2, S3, and S5 samples. Both the diameter of the circles and the color scale represent the fitness of the solution, with different scales to enhance visibility.

Table 3 Initial height, bi-axial/elastic modulus, and slackness factor obtained for the PI samples.

	S1 ($D_1\,t_1$)	S2 ($D_1\,t_1$)	S3 ($D_1\,t_1$)	S4 ($D_1\,t_2$)	S5 ($D_2\,t_2$)	S6 ($D_1\,t_1$)	S7 ($D_1\,t_3$)
Bi-axial modulus (GPa)	16	16	15.2	14.4	14.4	15.2	15.2
Elastic modulus (GPa) (*hp*. $\nu = 0.34$)	10.5	10.5	10	9.5	9.5	10	10
Initial height (mm)	0.145	0.15	0.14	0.10	0.16	0.21	0[a]
Slackness factor: $\frac{2\,h_i^2}{3\,r^2}$ (%)	0.041	0.043	0.039	0.020	0.022	0.039	0[a]

[a]Pre-stressed film.

The calculated elastic modulus for bare PI film ranges between 9.5 and 10.5 GPa, with an average value of 10 GPa (bi-axial modulus $M = 15.2$ GPa) for the 7 films and a standard deviation of 0.41 GPa. This value is considerably higher compared with the stiffer and thicker available PI commercial films (5 μm thick Kapton® EN datasheet reports $E = 5$ GPa with test method JIS K 7161), but it is supported by the literature investigating the mechanical properties variations between bulk and thin films.[7,8]

Because the FEA does not take into account any membrane anisotropy, the bi-axial modulus here found cannot be directly extended to the out-of-plane direction.

It is worth noting how the values of the initial height in Table 3 (that are a direct function of the slackness) are very close for samples coming from the same production batch (S1, S2, and S3) and with the same diameter.
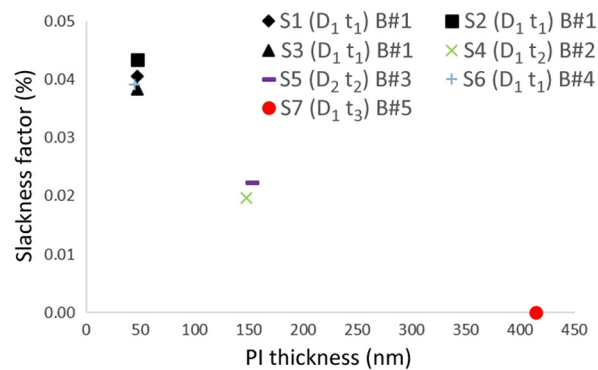
Fig. 7 Slackness factor trend versus thickness for bare PI membranes; in the legend, the color and shape of the marker indicate the batch and the sample number, respectively.

Looking at the slackness factor in Table 3, a correlation with the membrane thickness can be observed. A consistency on the slackness factor for membranes with the same thickness is shown with a value of 0.041 ± 0.002 for S1, S2, S3, and S6 (with $\sim$46 nm thickness) and a value of 0.021 ± 0.001 for S4 and S5 (with $\sim$150 nm thickness). The single, thicker S7 sample (with $\sim$415 nm thickness) shows signs of membrane pre-stress, thus resulting in a null slackness factor.

Looking at the graph in Fig. 7 where the slackness factor versus the PI thickness is reported, a decreasing trend of the slackness with the increase of the membrane thickness is found.

This behavior could be attributed to the manufacturing process (spin coating) combined with a possible different water absorption fraction for the thinner films in comparison with the thicker ones. The water diffusion in PI films is strongly dependent on the morphological structures in the films, which are remarkably sensitive to polymer chain rigidity and chemical backbone structure. Because, in this case, the stoichiometry of the PI is the same for all samples (BPDA/PPD $C_{22}H_{10}N_2O_4$), the reason for such phenomena may reside on the swelling mechanism due to the absorbed water that fills the free space within the polymer. Considering that the spin coating manufacturing process of PI determines different in-plane and out-of-plane strains during swelling,[39] it is reasonable to expect that this anisotropy would increase for thinner films. In Ref. 40, no variation of the elastic moduli was observed for PI films subjected to high humidity environments (85°C and 85% RH) after 6000 h of aging, but the tests were performed on relatively thick (50 μm) PI films.

The water absorption by thin PI films and its relevance on the mechanical properties may be the subject of a further study; however, it would require a modification of the experimental setup to perform deformation measurements under vacuum or alternatively by blowing N_2 atmosphere in a sample chamber.

4.2 PI Film Bulged Shape Comparison

Figure 8 shows a comparison between the experimental bulge profiles (at fixed pressures), the FEA profile (coming from the best-fit), and the circular arc approximation typically used for bulge tests, for the four geometries under study $(D_1\,t_1)$, $(D_1\,t_2)$, $(D_2\,t_1)$, and $(D_2\,t_2)$.

For each geometry, a couple of bulged profiles at different pressures are compared, one at low pressure and one at high pressure. In all cases, the FEA-simulated profiles fit very well the experimental profiles, confirming the validity of the experimental-numerical approach, whereas the circular arc approximation used for shape prediction on thin membranes is less accurate, especially near the border of the film.

4.3 PI-Al Coated Membrane Elastic Characterization

It is possible to obtain the elastic properties of the bilayer membrane, made by Al coated PI with different thicknesses and geometries (see Table 1), using the same experimental-numerical approach. Even if the substrate material (PI) is much less stiff than the coating (Al), its mechanical contribution cannot be neglected in the simulations. A bilayer model was used, with the previously found averaged bi-axial modulus of the PI ($M = 15.2$ GPa) serving as input for the new simulations, thereby determining the unknown Al properties.
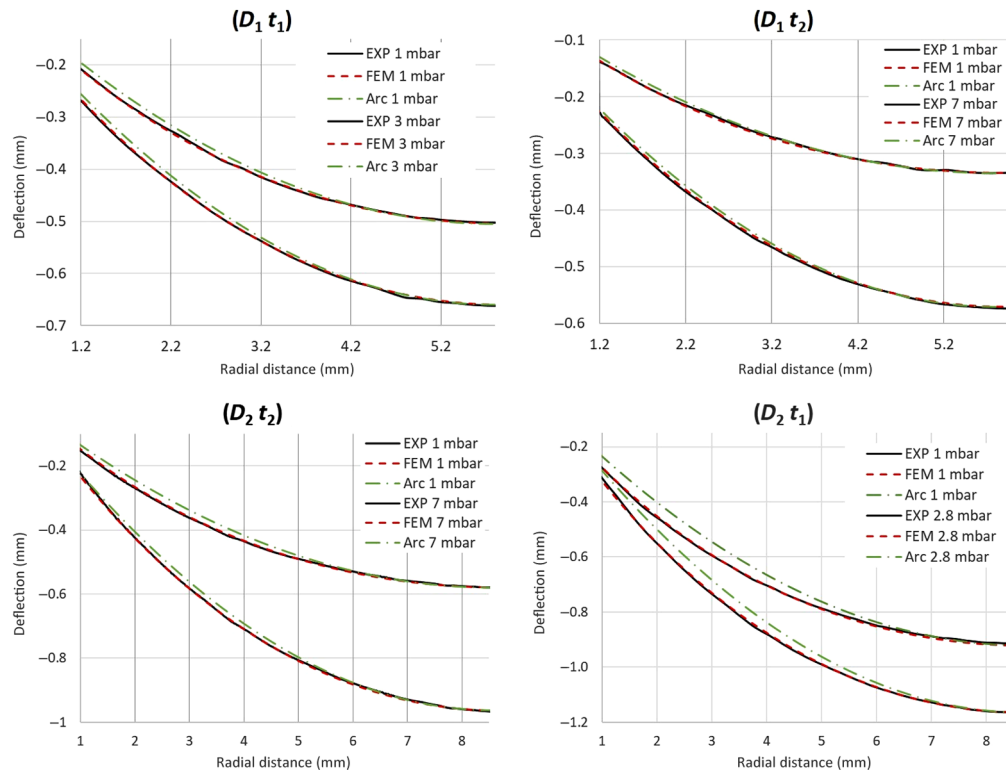
Fig. 8 Comparison of experimental (solid black), FEA simulated (dashed orange), and circular arc (dot-dashed green) profiles at a fixed pressure for the four sample geometries under study.

As an example, the Σ maps of the S4al sample are reported in Fig. 9.

The retrieved values for the elastic modulus, the initial height, and the slackness factor for the coated samples are summarized in Table 4.

The same considerations on the uncertainty must be done here for the elastic modulus retrieved on the aluminized sample in Table 4. It must be considered that, for a thinner Al coating (S1al, S2al, S3al, and S4al with $t = \sim 30$ nm), the uncertainty leads to a scattering in the elastic modulus of up to 15%. Thicker aluminized samples are much less affected by this uncertainty.
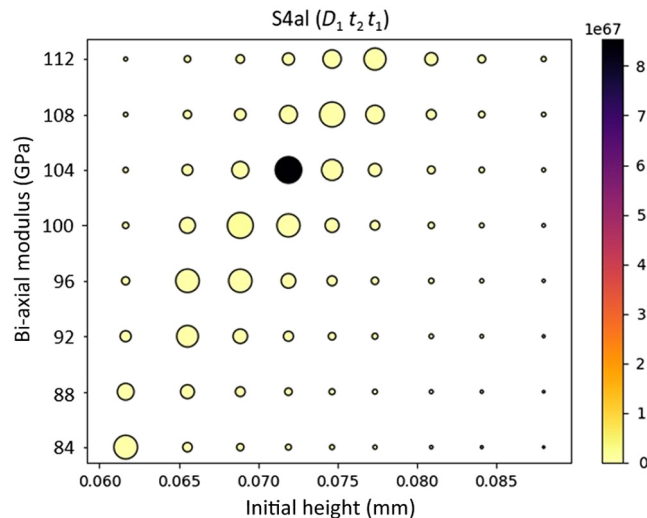
Fig. 9 Representation of Σ map for the S4al sample as a function of the Al coating elastic modulus and the film initial displacement. Both the diameter of the circles and the color scale represent the fitness of the solution, with different scales to enhance visibility.

Table 4 Initial height, bi-axial/elastic modulus, and slackness factor retrieved for the PI-Al coated samples.

	S1al $(D_1 t_1 t_1)$	S2al $(D_1 t_1 t_1)$	S3al $(D_2 t_2 t_1)$	S4al $(D_1 t_2 t_1)$	S5al $(D_1 t_2 t_2)$	S6al $(D_1 t_2 t_2)$	S7al $(D_1 t_2 t_3)$
Bi-axial modulus (GPa)	115	130	138	104	115	130	120
Elastic modulus (GPa) ($hp.\ \nu = 0.35$)	75	85	90	68	75	85	78
Initial height (mm)	0.077	0.072	0.112	0.072	0.077	0.079	0
Slackness factor: $\frac{2}{3}\frac{h_i^2}{r^2}$ (%)	0.011	0.010	0.012	0.010	0.011	0.012	0

For this reason, the values of the elastic modulus for the 4 thinner samples are scattered between 68 and 90 GPa. Even if the range seems relatively high, it is not unusual to find similar results in the literature for such a thin Al coating. In Ref. 38 a useful summary of the elastic modulus of Al thin films with different thicknesses collected by several authors is reported; it is worth mentioning that, with few exceptions (33 and 102 GPa), the values were found between 55 and 81 GPa with considerable scatter. In this work, the average value of the elastic modulus for all of the samples is equal to 79 GPa, with a standard deviation of 7.7 GPa.

The slackness factor for aluminized samples in Table 4 is found to be quite constant for all of the samples with the exception of the thickest one, S7al (with 152 nm of PI and 197 nm of Al), in which a flat membrane is observed at zero pressure. It is interesting to note that the slackness factor of the bare PI (see Table 3) is at least half the value of the aluminized one (with the exception of the thicker flat membranes S7 and S7al). This outcome reinforces our previous thoughts on the effect of the swelling on the PI film because, in this case, the polymer layer is constrained by a thicker and stiffer Al substrate that inhibits its expansion.

5 Conclusions

The plane strain bulge test is one of the best possible solutions for mechanical characterization of thin films, especially for freestanding membranes, but ultra-thin film tests are not a simple task due to arising residual stress and experimental uncertainty at very low pressure.

This work introduces a clear methodology for deriving the mechanical properties of ultra-thin membranes (thickness < 100 nm), combining the experimental measurements with a tailored set of numerical simulations. The novelty lies in the use of the initial height as the simulation parameter to fit the experimental data, which is necessary because, for the first time, we are dealing with ultra-thin PI films. The approach offers a broader range of applications, and its use under these challenging physical and numerical conditions demonstrates its reliability and stability.

The methodology was applied to find the elastic modulus of PI films (BPDA/PPD $C_{22}H_{10}N_2O_4$) with thicknesses in the range 50 to 400 nm and of Al coatings on PI with thicknesses in the range 30 to 200 nm.

An average elastic modulus of 10 GPa (standard deviation of 0.41 GPa) was found for the 7 tested bare PI films, a value that is higher than the commercial PI but is supported by the literature regarding the mechanical properties of thin films.[7,8] An average elastic modulus of 79 GPa (standard deviation of 7.7 GPa) was found for the Al coating.

The experimental and simulated bulged profile for the bare PI film was compared and showed a very good fit for all of the studied geometries, thus confirming the robustness of the experimental-numerical method.

Data Availability

The data that support the findings of this paper are not publicly available due to privacy. They can be requested from the author at nicola.montinaro@unipa.it.

Acknowledgments

References

1. M. Barbera et al., "ATHENA X-IFU thermal filters development status toward the end of the instrument phase-A," *Proc. SPIE* **10699**, 106991R (2018).
2. M. Barbera et al. "Thermal filters for the ATHENA X-IFU: ongoing activities toward the conceptual design," *J. Low Temp. Phys.* **184**(3–4) 706–711 (2016).
3. M. Barbera et al., "ATHENA WFI optical blocking filters development status toward the end of the instrument phase-A," *Proc. SPIE* **10699**, 106991E (2018).
4. D. Barret et al., "The ATHENA X-ray Integral Field Unit (X-IFU)," *Proc. SPIE* **9905**, 99052F (2016).
5. N. Meidinger et al., "The wide field imager instrument for Athena," *Proc. SPIE* **10397**, 103970V (2017).
6. S. Polak et al., "Design and acoustic tests of the ATHENA WFI filter wheel assembly development model towards TRL5," *J. Astron. Telesc. Instrum. Syst.* **9**(2), 024002 (2023).
7. E. Arzt et al., "Interface controlled plasticity in metals: dispersion hardening and thin film deformation," *Prog. Mater. Sci.* **46**(3), 283–307 (2001).
8. E. Eiper et al., "Size-independent stresses in Al thin films thermally strained down to −100°C," *Acta Mater.* **55**(6), 1941–1946 (2007).
9. Y. Xiang, X. Chen, and J. J. Vlassak, "Plane-strain bulge test for thin films," *J. Mater. Res.* **20**(9), 2360–2370 (2005).
10. M. K. Small and W. D. Nix, "Analysis of the accuracy of the bulge test in determining the mechanical properties of thin films," *J. Mater. Res.* **7**, 1553–1563 (1992).
11. C. K. Huang et al., "Mechanical properties of polymer thin film measured by the bulge test," *Thin Solid Films* **515**, 7222–7226 (2007).
12. R. Edwards, G. Coles, and W. Sharpe, "Comparison of tensile and bulge tests for thin-film silicon nitride," *Exp. Mech.* **44**, 49–54 (2004).
13. A. Karimi et al., "Characterisation of TiN thin films using the bulge test and the nanoindentation technique," *Thin Solid Films* **308**, 334–339 (1997).
14. M. K. Small, J. J. Vlassak, and W. D. Nix, "Re-examining the bulge test: methods for improving accuracy and reliability," *MRS Proc.* **239**, 257–262 (1991).
15. J. J. Vlassak and W. D. Nix, "A new bulge test technique for the determination of Young's modulus and Poisson's ratio of thin films," *J. Mater. Res.* **7**, 3242–3249 (1992).
16. I. Chasiotis, "Mechanics of thin films and microdevices," *IEEE Trans. Device Mater. Reliab.* **4**(2), 176–188 (2004).
17. W. C. Oliver and G. M. Pharr, "Measurement of hardness and elastic modulus by instrumented indentation: advances in understanding and refinements to methodology," *J. Mater. Res.* **19**(1), 3–20 (2004).
18. X. Li and B. Bhushan, "A review of nanoindentation continuous stiffness measurement technique and its applications," *Mater. Charact.* **48**(1), 11–36 (2002).
19. H. Ogawa et al., "Measurements of mechanical properties of microfabricated thin films," in *Proc. IEEE Tenth Annu. Int. Workshop on Micro Electro Mech. Syst. MEMS'97*, IEEE, pp. 430–35 (1997).
20. W. N. Sharpe, Jr., B. Yuan, and R. L. Edwards, "A new technique for measuring the mechanical properties of thin films," *J. Microelectromech. Syst.* **6**(3), 193–199 (1997).
21. B. Li et al., "Mechanics of morphological instabilities and surface wrinkling in soft materials: a review," *Soft Matter* **8**, 5728–5745 (2012).
22. D. K. Yang et al., "Sorption and transport studies of water in Kapton polymide," *J. Appl. Polym. Sci.* **30**(3), 1035–1047 (1985).
23. O. Tabata et al., "Mechanical property measurements of thin films using load-deflection of composite rectangular membranes," *Sens. Actuators* **20**, 135–141 (1989).
24. F. A. Marandi et al., "An experimental, analytical, and numerical investigation of hydraulic bulge test in two-layer Al–Cu sheets," *J. Manuf. Sci. Eng.* **139**(3), 031005 (2017).
25. H. Itozaki, "Mechanical properties of composition modulated copper-palladium foils," PhD Dissertation, Northwestern University (1982).
26. C. A. Neugebauer, J. B. Newkirk, and D. A. Vermilyea, *Structure and Properties of Thin Films*, John Wiley and Sons, New York, United States (1959).
27. A. Catlin and W. P. Walker, "Mechanical properties of thin single-crystal gold films," *J. Appl. Phys.* **31**(12), 2135 (1960).
28. R. Hill, "A theory of the plastic bulging of a metal diaphragm by lateral pressure," *Philos. Mag.* **41**(322), 1133–1142 (1950).

29. T. Tsakalakos, "The bulge test: a comparison of the theory and experiment for isotropic and anisotropic films," *Thin Solid Films* **75**(3), 293–305 (1981).

30. S. Timoshenko and S. Woinowsky-Krieger, *Theory of Plates and Shells*, p. 400, McGraw-Hill, New York, United States (1959).

31. T. Li and Z. Suo, "Ductility of thin metal films on polymer substrates modulated by interfacial adhesion," *Int. J. Solids Struct.* **44**(6), 1696–1705 (2007).

32. H. Wang et al., "Study on the effect of DIC deformation sensor on mechanical property of substrate," *Measurement* **49**, 283–288 (2014).

33. S. Bhandarkar et al., "Constitutive models for the viscoelastic behavior of polyimide membranes at ambient and deep cryogenic temperatures," *Fusion Sci. Technol.* **70**(2), 332–340 (2016).

34. N. Montinaro et al., "Deformation analysis of ATHENA test filters made of plastic thin films supported by a mesh under differential static pressure," in *IEEE 5th Int. Workshop on Metrol. for AeroSp. (MetroAeroSpace)*, pp. 393–397 (2019).

35. U. Lo Cicero et al., "Filters design and characterization for LAD instrument onboard eXTP," *Proc. SPIE* **12181**, 121816H (2022).

36. W. He et al., "Study on Young's modulus of thin films on Kapton by microtensile testing combined with dual DIC system," *Surf. Coatings Technol.* **308**, 273–279 (2016).

37. D. A. Grove, "Polyimide x-ray filter substrates optimized for cryogenic temperatures," *Proc. SPIE* **3766** (1999).

38. S. Lee, Y. Y. Kim, and Y. Cho, "A comparative study on the elastic characteristics of an aluminum thin-film using laser optical measurement techniques," *Coatings* **7**(9), 143 (2017).

39. N. C. B. Tan et al., "Interface effects on moisture absorption in ultrathin polyimide films," *J. Polym. Sci. B Polym. Phys.* **36**, 155–162 (1998).

40. S. Lahokallio, K. Saarinen, and L. Frisk, "Changes in water absorption and modulus of elasticity of flexible printed circuit board materials in high humidity testing," in *18th Eur. Microelectron. & Packag. Conf.*, Brighton, United Kingdom, pp. 1–6 (2011).

Nicola Montinaro is a mechanical engineer with a PhD in machine design awarded in 2015 in collaboration with the University of Cambridge with a thesis on mechanical characterization of nanostructured materials using new numerical approaches. From 2015 to 2018, he was a postdoc at the University of Palermo doing research on novel non-destructive evaluation techniques applied to composite structures, nanostructured materials, and metal additive manufactured parts. In 2018, he started an ongoing collaboration with the National Institute of Astrophysics (INAF-OaPA) to support the design, development, and mechanical characterization of thin membranes for x-ray observations. In 2020, he continued the collaboration on the same projects with a post doc at the University of Genève (UNIGE). Currently, he is a research fellow at the University of Palermo with an affiliation to INAF-OaPA, and he teaches a course on machine design. His main research interests include computational methods for engineering, nanostructured materials, non-destructive testing, and mechanical and thermo-mechanical characterizations of materials.

Ugo Lo Cicero received his PhD in electronic engineering and is a senior technologist at INAF. He works on the development of new technologies for astrophysics, in particular, related to x-ray instrumentation. He has worked on the design and development of microcalorimeter arrays, active optics, and x-ray sources and on the design and extensive characterization of cryogenic x-ray filters. He is a system manager for the "thermal filters" subsystem of the X-IFU instrument on board the ESA flagship mission Athena.

Fabio D'Anca received his master's degree in mechanical engineering in France in 2010. He is currently a technologist in INAF-Osservatorio Astronomico G.S. Vaiana, Palermo, Italy. He is involved in the design and mechanical characterization of very thin filters for the two detectors, WFI and X-IFU, on-board the ESA's Athena space mission, and of the IR optics of the ESA's ARIEL mission for the exploration of planetary atmospheres. His main expertize is in mechanical design, numerical modeling, and CNC fabrication of mechanical components.

Enrico Bozzo is currently research staff at the University of Geneva, Switzerland. His previous positions are: post-doc at the ISDC in 2009–2011; project manager of the LOFT mission in 2012–2014. Since 2014 he has been the Swiss project manager of: EUSO, Athena, Euclid, and THESEUS. His research interests are in high energy theoretical astrophysics, X- and Gamma-ray data analysis and interpretation, space instrumentation and science ground operations. He was involved in the following projects: INTEGRAL (science ground segment operations

coordinator from 2010 to present), LOFT (mission project manager, science ground segment definition coordinator), XIPE (mission project manager, project office), Athena (XIFU filter wheel & Swiss science ground segment project manager), Euclid (VIS/RSUproject manager), EUSO (LIDAR project manager) and THESEUS (ground segment lead, mission project manager, IRT filter wheel project manager).

Stéphane Paltani is full professor at the University of Geneva, Switzerland. His research interests are in AGN physics, AGN populations (multi-wavelength), cosmology, data analysis algorithms and interpretation, photometric redshifts. He was involved in the projects: INTEGRAL (science ground segment development), Chandra (archive scientist), Hitomi and XRISM (lead of the Swiss participation), Euclid (lead of the Swiss hardware and ground-segment activities, lead of the Photometric Redshift Organization Unit), MOONS (Co-PI), Athena (lead of the Swiss participation) and THESEUS (lead of the Swiss participation).

Marco Barbera received his PhD in physics in 1994. He has been an associate professor of astrophysics at Università degli Studi di Palermo, Italy, since 2004, and is affiliated with INAF-Osservatorio Astronomico G.S. Vaiana, Palermo, Italy, with responsibilities in setting-up and operating the x-ray astronomy calibration and testing (XACT) facility for the development and testing of instrumentation for x-ray astronomy missions (filters, optics, and detectors), such as Chandra, Newton-XMM, Hinode, Chang'E-1, and Coronas-Photons. He is presently co-I of the X-IFU instrument on board the ESA large mission Athena and is responsible for the design and development of the filters of its two detectors, X-IFU and WFI. He is also responsible for the design and development of the filters on board the NASA MIDEX solar mission MUSE.